Upper-mantle dynamics revealed by helium isotope variations along the southeast Indian ridge

D. W. Graham*, J. E. Lupton†, F. J. Spera‡ & D. M. Christie*

* *College of Oceanic & Atmospheric Sciences, Oregon State University, Corvallis, Oregon 97331, USA*
† *National Oceanic & Atmospheric Administration, Pacific Marine Environmental Laboratory, Hatfield Marine Science Center, Newport, Oregon 97365, USA*
‡ *Department of Geological Sciences, University of California, Santa Barbara, California 93106, USA*

Helium isotope variations in igneous rocks are important for relating isotopic heterogeneity to convective mixing in the Earth's mantle. High ^{3}He/^{4}He ratios at many ocean islands, along with lower and relatively uniform values in mid-ocean-ridge basalts (MORBs), are thought to result from a well mixed upper-mantle source for MORB and a distinct deeper-mantle source for ocean island basalts[1]. At finer scales, ^{3}He/^{4}He variations along mid-ocean ridges have been related to underlying mantle heterogeneity[2,3], but relationships between the scales of geochemical segmentation and mantle convection remain enigmatic. Here we present helium isotope data for MORB glasses recovered along ~5,800 km of the southeast Indian ridge, and develop an approach to quantitatively relate spatial variations in geochemical and geophysical parameters at the Earth's surface. A point-to-point correlation analysis reveals structure in the helium isotope data at length scales of ~150 and ~400 km that appears to be related to secondary convection in the underlying mantle.

The southeast Indian ridge (SEIR; Fig. 1) stretches from the Rodrigues triple junction (25.6 °S, 70.1 °E) to the Macquarie triple junction (62 °S, 151 °E). Between 76° and 78° E it crosses the Amsterdam–St Paul plateau (ASP), a pronounced swell associated with relatively hot mantle upwelling beneath Amsterdam and St Paul islands[3], while between 120° and 128 °E it crosses the Australian–Antarctic discordance (AAD), a region of deep bathymetry (≈ 4,000 m) associated with relatively cold mantle and low melt production[4]. From 88° to 120 °E, the increase in depth of the ridge axis, and the morphological transition from an axial high to an axial valley, imply that melt production rate and crustal thickness decrease eastwards along axis, despite the relatively constant full spreading rate of 70–75 mm yr^{-1} (ref. 5). On the basis of petrologic analyses of more than 3,000 basalt glasses[6–9], there is an inferred gradient in mantle temperature of ~80–150 °C from east to west. The hottest mantle is present beneath the ASP, and the coldest mantle beneath the AAD region. Given the constant spreading rate and the absence of large transform offsets and nearby hotspots, this portion of the SEIR provides a unique opportunity to study the geochemical consequences of along-axis variations in upper-mantle temperature.

We analysed helium isotopes following *in vacuo* crushing of basalt glass[10], and report the helium isotope composition relative to the atmospheric ^{3}He/^{4}He ratio (R_A). (Data are available as Supplementary Information.) Variations in ^{3}He/^{4}He, axial depth and Fe_8 are shown against distance along the SEIR in Fig. 2. (Fe_8 is the FeO content in wt%, corrected for crystal fractionation to 8% MgO, and may be used as an indicator of the mean depth of mantle melting[11]). Between distances of ~1,000 and 3,000 km east of the ASP (that is, from the axial depth minimum at 88° E to the AAD; Fig. 2), there is a long-wavelength eastward decrease in ^{3}He/^{4}He and Fe_8, and an increase in axial depth which may trace sub-ridge mantle flow down a thermal gradient[5]. Near the ASP, ^{3}He/^{4}He ratios extend above 14 R_A due to the presence of the Amsterdam–St Paul hotspot[3]. In the AAD, ^{3}He/^{4}He ratios are as low as 6.2 R_A, and are among the lowest values yet observed in MORB away from the influence of subduction zones[12].

There is a good ^{3}He/^{4}He–Fe_8 covariation along much of the SEIR. Because the peaks in ^{3}He/^{4}He and Fe_8 do not occur in precisely the same locations, we computed Spearman's rank correlation coefficient (r_s) as a non-parametric test of the significance of the correlation. We excluded samples on top of the ASP to remove hotspot effects. For the remaining data ($n = 91$) $r_s = 0.65$, well above the critical value of 0.21 for a 0.05 significance level (in a two-tailed test with 90 degrees of freedom), and so the null hypothesis that the ^{3}He/^{4}He–Fe_8 relationship is random can be rejected. The covariation of ^{3}He/^{4}He and Fe_8 therefore suggests that higher ^{3}He/^{4}He is associated with a higher mean pressure of melting[11]. One possible explanation for the ^{3}He/^{4}He–Fe_8 covariation is a layered upper mantle having higher ^{3}He/^{4}He ratios at depth. Mantle which is

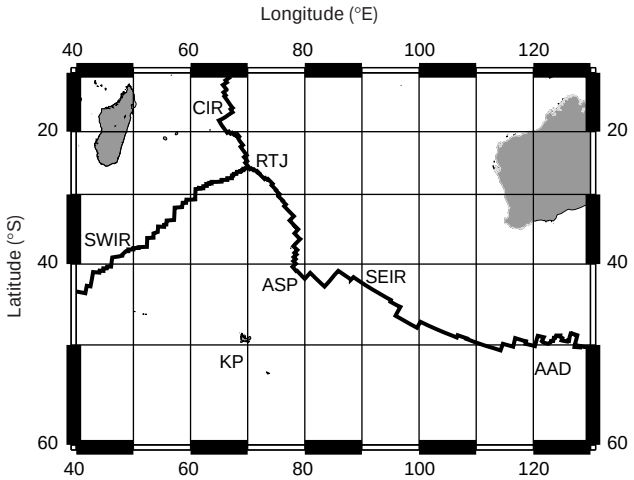

Figure 1 Location map of Indian Ocean features. SEIR, southeast Indian ridge; SWIR, southwest Indian ridge; CIR, central Indian ridge; RTJ, Rodrigues triple junction; ASP, Amsterdam–St Paul plateau; AAD, Australian–Antarctic discordance; KP, Kerguelen plateau.

hotter and begins to melt deeper will produce aggregated MORB melts having higher values of Fe_8 (ref. 11). According to this first explanation, $^3He/^4He$ values will also be higher due to a proportionally greater sampling of the deep upper mantle. Another possible origin for the $^3He/^4He$–Fe_8 covariation is from melting of discrete heterogeneities, having lower solidus temperatures, that are embedded within upper-mantle peridotite. Such heterogeneities could, for example, occur as blobs or veins of garnet pyroxenite having low $^3He/^4He$, due to their origin from recycled crust[13]. Garnet pyroxenite melts preferentially to surrounding mantle peridotite. However, its contribution to erupted basalt is significantly less when magma genesis begins at a higher mantle temperature and pressure, because the pyroxenitic melts become effectively diluted by partial melts of peridotite[14]. According to this second explanation, hotter mantle would begin to melt deeper and would also lead to aggregated MORB melts that have higher values of Fe_8 and $^3He/^4He$. This model implies that some highly depleted (pyroxenite-free) regions of the upper mantle may have $^3He/^4He$ ratios above 9 R_A. One of the few examples of such high $^3He/^4He$ ratios in ultra-depleted MORB glass comes from the Garrett transform on the southern East Pacific Rise[15], where a MORB lava with $\epsilon_{Nd} = +11$ has $^3He/^4He = 9.7\ R_A$.

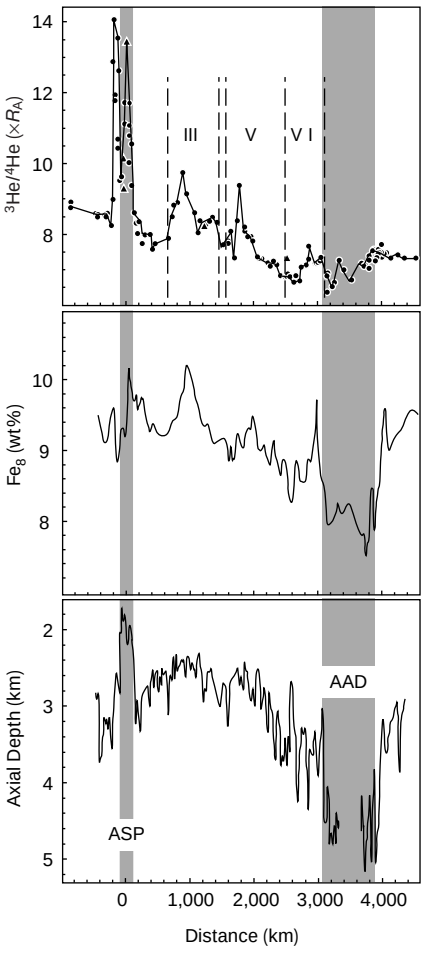

Figure 2 $^3He/^4He$, Fe_8 and axial depth versus distance along the SEIR. Basalt glasses have been recovered from the SEIR by a number of seagoing expeditions. From segments immediately northwest of the Amsterdam–St Paul plateau (ASP) to the Australian–Antarctic discordance (AAD), all sampling has been precisely located in the neovolcanic zone based on multi-beam bathymetry and magnetic surveys. Average sample density for $^3He/^4He$ across this region of ~4,000 km is 1 sample every 45 km. Distance is calculated from the pole of plate rotation (13.2° N, 38.2° E)[29] and is shown relative to St Paul Island (38.70° S, 77.55° E). The ASP and AAD regions are depicted as shaded bands. The dashed lines and roman numerals delineate the zero-order tectonic segmentation from satellite gravity analysis[16]. The line shown for Fe_8 is the five-point running mean. Triangles represent lavas from seamounts and off-axis lava fields. Helium isotope data are from this study and from refs 3 and 30.

Superimposed on the long-wavelength gradients along the SEIR, there are several peaks in $^3He/^4He$ and Fe_8 that range between 200 and 500 km in basal width (Fig. 2). These peaks are most prominent near the ASP, and at 88° E, 97° E and 111° E (at along-axis distances of 910, 1,800 and ~2,850 km, respectively; Fig. 2). The latter three peaks occur near the centres of the zero-order, regional segmentation of the ridge (Fig. 2) defined by the persistence of fracture zone anomalies in satellite gravity data. This segmentation reveals several coherent tectonic units, up to ~900 km in along-axis width, that have been stable since reorientation of the SEIR when it migrated over the Kerguelen plume 38 Myr ago (ref. 16).

To evaluate quantitatively the length scales of helium isotope variation along the SEIR, we applied a spatial correlogram analysis, similar to approaches used previously to study magma mixing[17]. The correlation coefficient R is calculated between every pair of points at a separation distance r. For each point pair, $R(r)$ is given by the product of the deviations in $^3He/^4He$ from the population mean, normalized to the population variance[18]. For n sample points, the total number of point pairs is $N = n(n-1)/2$; for the 120 sample localities along the SEIR there are 7,140 sample pairs. A value of $R(r)$ close to 1 indicates that a $^3He/^4He$ value above the population average at a given location is likely to be associated with an above-average value at a distance r away. (Similar arguments hold for below-average values.) $R(0)$ is equal to unity by definition. A value of $R(r)$ close to zero implies a random relationship between $^3He/^4He$ values at points located a distance r apart. A value of $R(r)$ close to -1 implies an anticorrelated relationship. For any mixture which is not perfectly homogeneous, $R(r)$ will be greater than 0 at small values of r because points close together will usually be from the same "clump"[18]. The lowest value of r at which $R(r)$ goes to zero is denoted as r^*.

The correlogram ($R(r)$ versus r) can be used to define a scale of segregation[18] similar to conceptualizations for the scale of turbulence in fluid flow[19]. The scale of segregation, L, is the integral of $R(r)$ from $r = 0$ to $r = r^*$, and is related to the size of clumps within a mixture. Within the Earth's interior, such clumps must vary in size and shape and their boundaries may be diffuse[20]. We have no *a priori* information on their dimensions, so it is not possible to refer to an 'average size' of clumps. We introduce the L concept because it is a quantitative estimate of size that can be precisely defined from spatially referenced geochemical data. (We note that there are three dominant 'scales of mantle convection' inferred from seismic tomography, topography and gravity studies[21]. These dominant length scales occur at spherical harmonics degree 2 (~16,000 km) and degree 6 (~6,000 km), and at a smaller scale between 400 and 1,000 km. The length scales of geochemical variation in the mantle should be related to these convective scales, although not necessarily in a one-to-one manner.)

The correlogram method is strictly only applicable to stationary data; that is, data which show no trend in mean level over the length of observation. Because there is a long-wavelength gradient in the $^3He/^4He$ baseline along the central portion of the SEIR, we applied the spatial correlogram approach both to the measured $^3He/^4He$ ratios, and to computed regression residuals from a linear fit of $^3He/^4He$ versus along-axis distance. Both the correlogram for the $^3He/^4He$ results and that for the residuals show the expected decrease in $R(r)$ with separation distance (Fig. 3). The values of r^* and L for the raw data are 1,600 km and 620 km, respectively, but these estimates are strongly affected by the existence of the regional $^3He/^4He$ gradient, as confirmed by simple forward models. For the 'detrended' data (that is, the regression residuals) r^* and L are ~400 km and ~150 km, respectively. These distances accurately

reflect the length scales of $^3He/^4He$ variation that are qualitatively discernible within the regional trend along the SEIR (Fig. 2).

Because these values of r^* and L are significantly larger than the average sampling density of ~45 km, they do not represent random variations. The value of $r^* = 400$ km resembles the largest scale (zero order) tectonic segmentation of the ridge, delineated by fracture zones that have persisted throughout the spreading history of the SEIR[16]. Length scales of the order of 10^2 km are similar to those of hypothetical, secondary convective 'cells' in the underlying mantle. For example, undulations in the geoid for the Pacific plate, ranging in wavelength from 200 km near the ridge to 400–600 km far away, have previously been ascribed to convective rolls in the uppermost mantle[22,23]. Such cellular structures would be aligned roughly orthogonal to the ridge axis. If such secondary convection is present beneath the SEIR, its geometry may be a remnant from the passage of the ridge over the Kerguelen plume about 38 Myr ago (ref. 24), similar to features that form in the wake of plumes in numerical models of mantle convection[25]. Alternatively, secondary convection might result from a thermal feedback induced by fracture zones, where patterns of upper-mantle convection are established during the initiation of spreading or continental breakup. A further possibility is that it might simply be an intrinsic feature of the inferred eastward mantle flow toward the AAD in this part of the Indian Ocean, the so-called "Richter rolls"[26].

Mantle convection is undoubtedly unsteady on a geological timescale. The simplest form of this unsteadiness is one in which convective cells oscillate or pulsate slightly[27]. Significantly, this tends to produce some lateral mass transport between cells. Based on our correlogram analysis, the characteristic length scale for tracer (helium) transport is of the order of 150–400 km in this region of the Indian Ocean mantle. 'Mixing' within cells of this length would be significantly faster than 'dispersion' between cells, and the relative importance of these transport phenomena would mainly depend on the regional Rayleigh number.

Our results provide good evidence for some control of along-axis geochemical variations by secondary convection patterns in the upper mantle. Spatial correlogram analysis provides a way to investigate geochemical variations at local, regional and global scales; this technique also has the potential to link quantitatively such variations to geophysical patterns—such as those detected with seismic tomography[28]. □

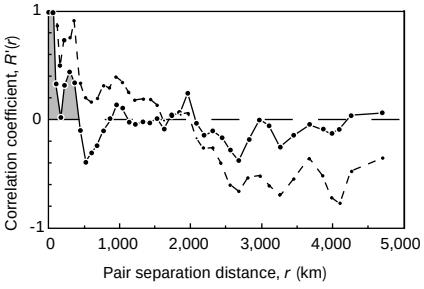

Figure 3 Spatial correlogram for $^3He/^4He$ variations along the SEIR. The correlation coefficient $R(r)$ is

$$R(r) = \frac{\overline{(c_i - \bar{c})(c_j - \bar{c})}}{\sigma^2}$$

where c_i and c_j are the $^3He/^4He$ ratios at locations i and j, respectively, $\bar{c}$ is the population mean, σ^2 is the population variance, r is the distance between points i and j, and the overbar designates an ensemble average over all pairs. The mean value of $R(r)$ has been plotted for a constant number of point pairs per distance interval. This constant population method produces similar results to one using bins of constant width, but provides a more robust correlogram at large r. The correlograms shown are for the full data set, with 120 sample locations (7,140 point pairs) and $r_{max} = 5{,}843$ km, using 40 distance bins each with 178 members. The mean $^3He/^4He$ is 8.30 R_A, and the variance is 2.43 R_A. The dashed line shows the correlogram for the raw $^3He/^4He$ data, and the solid line shows the correlogram for regression residuals in which the regional $^3He/^4He$ gradient has been removed by a linear fit. For this detrended $^3He/^4He$ case, the segregation length scale (L) shown by the shaded area is ~150 km, and r^* (see text) is ~400 km.

Received 10 February; accepted 11 December 2000.

1. Lupton, J. E. Terrestrial inert gases: isotope tracer studies and clues to primordial components in the mantle. *Annu. Rev. Earth Planet. Sci.* **11,** 371–414 (1983).
2. Lupton, J. E., Graham, D. W., Delaney, J. R. & Johnson, H. P. Helium isotope variations in Juan de Fuca Ridge basalts. *Geophys. Res. Lett.* **20,** 1851–1854 (1993).
3. Graham, D. W., Johnson, K. T. M., Priebe, L. D. & Lupton, J. E. Hotspot-ridge interaction along the Southeast Indian Ridge near Amsterdam and St. Paul Islands: helium isotope evidence. *Earth Planet. Sci. Lett.* **167,** 297–310 (1999).
4. Sempéré, J.-C., Palmer, J., Christie, D., Morgan, J. P. & Shor, A. Australian-Antarctic Discordance. *Geology* **19,** 429–432 (1991).
5. Sempéré, J.-C., Cochran, J. R. & Team, S. S. The Southeast Indian Ridge between 88°E and 118°E: variations in crustal accretion at constant spreading rate. *J. Geophys. Res.* **102,** 15489–15505 (1997).
6. Klein, E. M., Langmuir, C. H. & Staudigel, H. Geochemistry of basalts from the South East Indian Ridge, 115°E-138°E. *J. Geophys. Res.* **96,** 2089–2107 (1991).
7. Pyle, D. G. *Geochemistry of mid-ocean ridge basalt within and surrounding the Australian Antarctic Discordance.* PhD thesis, Oregon State Univ. (1994).
8. Douglas Priebe, L. M. *Geochemical and petrogenetic effects of the interaction of the Southeast Indian Ridge and the Amsterdam-St. Paul hotspot.* MS thesis, Oregon State Univ. (1998).
9. Sours-Page, R. *Magmatic processes at mid-ocean ridges: evidence from lavas and melt inclusions from the Southeast Indian Ridge, East Pacific Rise and Juan de Fuca Ridge.* PhD thesis, Oregon State Univ. (2000).
10. Graham, D., Lupton, J., Albarède, F. & Condomines, M. Extreme temporal homogeneity of helium isotopes at Piton de la Fournaise, Réunion Island. *Nature* **347,** 545–548 (1990).
11. Klein, E. M. & Langmuir, C. H. Global correlations of ocean ridge basalt chemistry with axial depth and crustal thickness. *J. Geophys. Res.* **92,** 8089–8115 (1987).
12. Sturm, M. E., Klein, E. M., Graham, D. W. & Karsten, J. Age constraints on crustal recycling to the mantle beneath the southern Chile Ridge: He-Pb-Sr-Nd isotope systematics. *J. Geophys. Res.* **104,** 5097–5114 (1999).
13. Allègre, C. J. & Turcotte, D. L. Implications of a two-component marble-cake mantle. *Nature* **323,** 123–127 (1986).
14. Hirschmann, M. M. & Stolper, E. M. A possible role for garnet pyroxenite in the origin of the "garnet signature" in MORB. *Contrib. Mineral. Petrol.* **124,** 185–208 (1996).
15. Mahoney, J. J. *et al.* Isotope and trace element characteristics of a super-fast spreading ridge: East Pacific Rise, 13-23°S. *Earth Planet. Sci. Lett.* **121,** 173–193 (1993).
16. Small, C., Cochran, J. R., Sempéré, J.-C. & Christie, D. M. The structure and segmentation of the Southeast Indian Ridge. *Mar. Geol.* **161,** 1–12 (1999).
17. Oldenburg, C. M., Spera, F. J., Yuen, D. A. & Sewell, G. Dynamic mixing in magma bodies: theory, simulations, and implications. *J. Geophys. Res.* **94,** 9215–9236 (1989).
18. Danckwerts, P. V. The definition and measurement of some characteristics of mixtures. *Appl. Sci. Res.* **3,** 279–296 (1952).
19. Taylor, G. I. Statistical theory of turbulence: Parts 1-4. *Proc. R. Soc. Lond. A* **151,** 421–478 (1935).
20. Gurnis, M. Stirring and mixing in the mantle by plate-scale flow: large persistent blobs and long tendrils coexist. *Geophys. Res. Lett.* **13,** 1474–1477 (1986).
21. Anderson, D. L. The scales of mantle convection. *Tectonophysics* **284,** 1–17 (1998).
22. Haxby, W. F. & Weissel, J. K. Evidence for small-scale convection from Seasat altimeter data. *J. Geophys. Res.* **91,** 3507–3520 (1986).
23. Baudry, N. & Kroenke, L. Intermediate-wavelength (400-600 km), South Pacific geoidal undulations: their relationship to linear volcanic chains. *Earth Planet. Sci. Lett.* **102,** 430–443 (1991).
24. Duncan, R. A. & Storey, M. in *Synthesis of Results from Scientific Drilling in the Indian Ocean* (eds Duncan, R. A., Rea, D. K., Kidd, R. B., von Rad, U. & Weissel, J. K.) 91–103 (Geophysical Monograph 70, American Geophysical Union, Washington DC, 1992).
25. van Keken, P. E. & Gable, C. W. The interaction of a plume with a rheological boundary: a comparison between two- and three-dimensional models. *J. Geophys. Res.* **100,** 20291–20302 (1995).
26. Richter, F. M. & Ribe, N. M. On the importance of advection in determining the local isotopic composition of the mantle. *Earth Planet. Sci. Lett.* **43,** 212–222 (1979).
27. Camassa, R. & Wiggins, S. Transport of a passive tracer in time-dependent Rayleigh-Bénard convection. *Physica D* **51,** 472–481 (1991).
28. Kellogg, L., Hager, B. & van der Hilst, R. Compositional stratification in the deep mantle. *Science* **283,** 1881–1884 (1999).
29. Gripp, A. E. & Gordon, R. G. Current plate velocities relative to the hotspots incorporating the NUVEL-1 global plate motion model. *Geophys. Res. Lett.* **17,** 1109–1112 (1990).
30. Graham, D., Lupton, J., Klein, E., Christie, D. & Pyle, D. in *Proc. 7th Int. Conf. on Geochronology, Cosmochronology and Isotope Geology*, Vol. 27, 41 (Geological Society of Australia, Sydney, 1990).

Supplementary information is available on *Nature*'s World-Wide Web site (http://www.nature.com) or as paper copy from the London editorial office of *Nature*.

Acknowledgements

We thank G. Brown for computer code development, and M. Fisk, B. Hanan, G. Ito, J. Mahoney and D. Pyle for discussions. This work was supported by the NSF, the US DOE, and the NOAA Vents Program.

Correspondence and request for materials should be addressed to D.W.G. (email: dgraham@oce.orst.edu).

New Helium Isotope Results for SEIR Basalt Glasses, 88°-118°E

Sample	Segment / Location	Latitude (°S)	Longitude (°E)	Depth (m)	$^3He/^4He$ (R/R_A)	2σ	[He] (μccSTP/g)
BMRG06 33-1	L	42.115	88.042	2450	9.70	0.05	16.32
BMRG06 35-8	L	41.322	86.632	2560	8.86	0.06	0.306
WW10 69-1	C17	41.870	88.922	2353	9.14	0.05	3.70
WW10 70-32	C16	42.570	90.187	2575	8.61	0.05	11.78
WW10 71-1	C16	42.886	90.795	2350	8.02	0.04	5.45
WW10 72-2	C16 smt	43.417	91.283	1470	8.21	0.06	1.24
WW10 65-9	C16	43.082	91.095	2494	8.35	0.04	2.30
WW10 73-8	C16	43.468	91.684	2738	8.24	0.05	1.85
WW10 75-4	C15	43.575	92.662	2610	8.37	0.04	10.72
WW10 76-1	C15	43.882	93.114	2653	8.46	0.04	12.33
WW10 77-7	C15	44.117	93.773	2795	8.34	0.04	7.74
WW10 78-2	C14	44.833	94.833	2719	7.71	0.04	11.41
WW10 81-1	C14	45.174	95.590	3190	7.81	0.06	0.54
WW10 82-35	C14 rift tip	45.185	95.585	3180	7.75	0.04	10.40
WW10 84-7	C14 transform	45.111	95.932	2580	8.08	0.04	4.44
WW10 WC48	C13/14	46.090	95.926	2990	7.31	0.04	0.99
WW10 87-38	C13	46.778	96.368	2520	8.37	0.05	0.88
WW10 88-1	C13	47.076	96.833	2568	9.38	0.05	6.30
WW10 89-4	C13	47.445	97.512	2450	8.08	0.05	1.65
WW10 89-107	C13				8.33	0.05	4.05
WW10 90-1	C13	47.711	98.157	2570	7.90	0.04	10.45
WW10 91-3	C13	47.909	98.601	2900	7.92	0.04	1.83
WW10 92-1	C13	48.101	98.943	2668	7.82	0.04	2.28
WW10 96-1	C12	47.335	100.672	2465	7.36	0.04	2.74
WW10 98-3	C12	47.458	100.961	2583	7.33	0.04	3.78
WW10 100-1	C12	47.630	101.530	2850	7.32	0.04	17.77
WW10 103-4	C12	48.019	102.540	3230	7.18	0.04	3.76
WW10 106-4	C11	47.878	103.353	2950	7.12	0.04	13.82
WW10 110-4	C11	48.103	103.930	3410	7.25	0.04	4.65
WW10 111-18	C10	48.212	104.662	3015	7.16	0.04	12.54
WW10 113-7	C9	48.752	105.224	3630	6.82	0.04	0.83
WW10 114-12	C9 smt	49.116	105.588	2875	7.36	0.04	4.84
WW10 115-3	C9	49.229	105.868	3696	6.80	0.04	7.52
WW10 116-15	C9/8 transform	48.873	106.494	4835	6.82	0.06	3.24
WW10 117-1	C8	48.348	107.145	3520	6.88	0.04	8.78
WW10 118-1	C8	48.428	107.527	2673	6.80	0.04	6.48
WW10 122-1	C8	48.700	108.200	3255	6.65	0.04	2.11
WW10 124-1	C7 transform	49.025	108.513	3935	6.83	0.04	3.53
WW10 125-1	C7	49.450	109.105	3440	6.68	0.03	15.94
WW10 126-1	C7	49.527	109.484	3240	7.07	0.04	6.49
WW10 128-1	C7	49.828	110.412	2745	7.13	0.05	0.64
WW10 128-18	C7				7.70	0.04	5.81
WW10 130-1	C6	49.775	111.133	3515	7.30	0.04	6.89
WW10 134-1	C5	50.295	112.490	3620	7.20	0.04	11.97
WW10 135-8	C5 rift tip	50.307	112.593	3748	7.20	0.04	15.30
WW10 138-1	C4	50.187	112.855	3820	7.28	0.04	11.60
WW10 140-5	C4	50.300	113.453	3320	7.26	0.04	0.52
WW10 141-1	C4	50.347	113.615	3002	7.35	0.04	3.04
WW10 144-4	C3	50.007	115.212	3997	6.84	0.04	8.09
WW10 145-1	C3	49.273	116.717	4610	6.53	0.03	15.82
WW10 145-7	C3				7.20	0.08	2.52
WW10 146-1	C2	49.505	117.182	4755	6.65	0.04	5.02

All analyses are for the helium trapped in vesicles, which was released by *in vacuo* crushing of glass chunks several mm in size. Reported uncertainties in $^3He/^4He$ are the quadrature sum of analytical error in air standards, samples and blanks. The He peak height in air standards is reproducible to <1%; uncertainties in sample He contents are larger, however, primarily due to inhomogeneities in vesicle distribution.